Spray wall interaction: study of preferential vaporization of fuel film as function of injection pressure and wall temperature

Anthony Roque*[1], Fabrice Foucher[1], Jerome Helie[2]
[1] Université d'Orléans, Orléans, France
[2]Continental Automotive SAS, Toulouse, France
*Corresponding author: anthony.roque@univ-orleans.fr

Abstract
The preferential vaporization of a multi-component fuel was studied by laser-induced fluorescence of two aromatic tracers. The spatial distribution of the light-medium and heavy components were studied after the spray-wall interaction. The experimental condition abroad low and high values of injection pressure and wall temperature. The temperature range of study was from 80 °C to 200 °C. Three values of injection pressure were used: 30, 100 and 200 bar.

Keywords
Preferential vaporization, fluorescence, Gasoline Direction Injection engines, fuel film.

Introduction
Downsizing and Direct Injection (DI) implementation were two main trends in the gasoline engine development for the last decade and many new challenges came with them. Currently, the gasoline direct injection (GDI) engines are growing fast in the U.S. market place representing more than 50% of vehicles produced in 2017 [1]. Considering the European market, the same trend was observed [2]. The Real Driving Emissions (RDE) requirements, for Euro 6 passenger cars and vans, is far from perfect, and work is underway to identify current shortcomings to enable future improvements [3]. One of the main challengers on RDE conditions is the spray-wall interaction, because the extreme conditions of the tests, such as cold start. Under this conditions liquid fuel wall films are generated on the combustion chamber due to significantly reduction of fuel evaporation, constituting in a significant source of PN emissions in GDI engines [4,5].
Spray-wall interaction in a real engine involves many parameters, such as the operational regime of the engine (load and speed), the injection strategy, injection pressure, the nature (roughness, chemical composition) and temperature of the wall, physico-chemical properties of the fuel, and the ambient conditions [6,7]. Additionally, the local distribution and the composition of the fuel film, which is generated after the spray-wall interaction, could have a high influence in the soot generated from pool fires during combustion in GDI engines [8,9].
In order to know the effect of the injection pressure and the wall temperature on the distribution of the light-medium and heavy fraction of a multicomponent fuel on a fuel film, the vaporization process around the impingement region was analysed inside a controlled environment, which was carried on inside a constant volume vessel (CVV). To achieve this aim, the new methodology presented by Itani et al. [10] and validated by Bardi et al. [11] was used. This methodology involves to measure the fluorescence of two different traces (1,4 Difluorobenzene and 1-Methylnaphthalene), which were used to follows the light and heavy fractions during the vaporization process.

Material and methods
The preferential vaporization was analysed inside a constant volume vessel of 4 litres (Figure 1a), where a one hole injector was installed to permit the direct impact of the spray on an aluminium plate. The angle of impact is approximately 33 degrees, respect plate surface. The setup features can be found in [8]. The experimental conditions of the test are presented in the Table 1; the initial equivalence ratio (ϕ_0) is increased after the injection to 0.98. As can be seen, the parameters that will be analysed are the injection pressure (P_{Inj}) and the wall temperature (T_{wall}). The mass of injected fuel is independent of the pressure increase. The main properties of each components of the gasoline surrogate are presented in in the Table 2, as well as its composition (hexane, iso-octane and dodecane). The two tracer used are: 1-MethylNaphthalene (1-MN) and 1,4 DifluorBenzene (DFB); their properties are presented in the Table 3. The first one is used as tracer of the heavy fraction and the second one to light-medium fraction. A transparent gasoline surrogate was used in order to no interfere in the emission spectrum of the tracers. The verification of fluorescent impurities of each component, which can overlap the fluorescence of dopants, was performed using a Photonic multichannel analyzer (Hamamatsu C10029). Figure 2 shows the fluorescence spectra for each component and the surrogate with the dopants, the values were dimensionless using the peak value of the laser signal at 266 nm. A small signal of florescence was identified for each component, but

This work is licensed under a Creative Commons 4.0 International License (CC BY-NC-ND 4.0).

theirs interference compared to the fluorescence signal of the surrogate with dopants is negligible. Figure 2 also shows the range of signal collected for DFB and 1-MN. The acquisition of each single test provide three reference images (Im1, Im2, Im3) before the injection event and one with the vaporization process (Im4), as it can be observed on the Figure 1b. The acquisition timing for the vaporization was stablished based on the end of injection (EOI) and four different times (t_{EOI}) were selected: 4.1; 15.1; 26.1 and 38.1 ms. The acquisition period goes from the time when fuel spray pass to vapour phase until the arrive of the flame front. The first timing was obtained using Mie scattering of spray and the second one comes from the Schlieren images for flame front propagation in a reactive experiment. The main timing values were stablished in previous works [8,12]. The reference images permitted to identify the irregularities in the vapour distribution due to the flow movements around the plate and correct the intensity signal due to the temperature gradients. The Figure 1c presents the optical arrangement to produce a light sheet (at 266 nm). The signal of fluorescence was acquired using an image doubler (La Vision) mounted on ICCD camera, the image doubler permit to capture two images in simultaneous and each channel was used to capture the signal of 1-MN (filter combination: 20CGA320/ZUS0350) and DFB (filter combination: ZUL0275/ZUS0300). Figure 3a summarizes the post-processing of the images until obtain the 2D maps to be analysed in results section. The calibration used different 2D images for four ϕ values to correct the irregularities of the light sheet and the level of intensities of each channel captured for the image doubler (pixel-to-pixel calibration). Additionally, other set of images where captured for the same ϕ values but changing the energy of the laser, with this data will be possible to leave the fluorescent signal independent of the laser energy before the calibration with the concentration maps (ϕ). The level of energies used was below the saturation threshold; at this condition, the fluorescence intensity is proportional to the laser energy. The interference of the flow patterns generated for the temperature gradients were reduced obtaining the ratio between the Im4 and the average of the reference images (Im1, Im2 and Im3), Figure 3b. For ensuring a better representability of the results, each test was repeated 6 times and the average results are analysed. More details of the calibration process and the experimental setup can be found in [12].

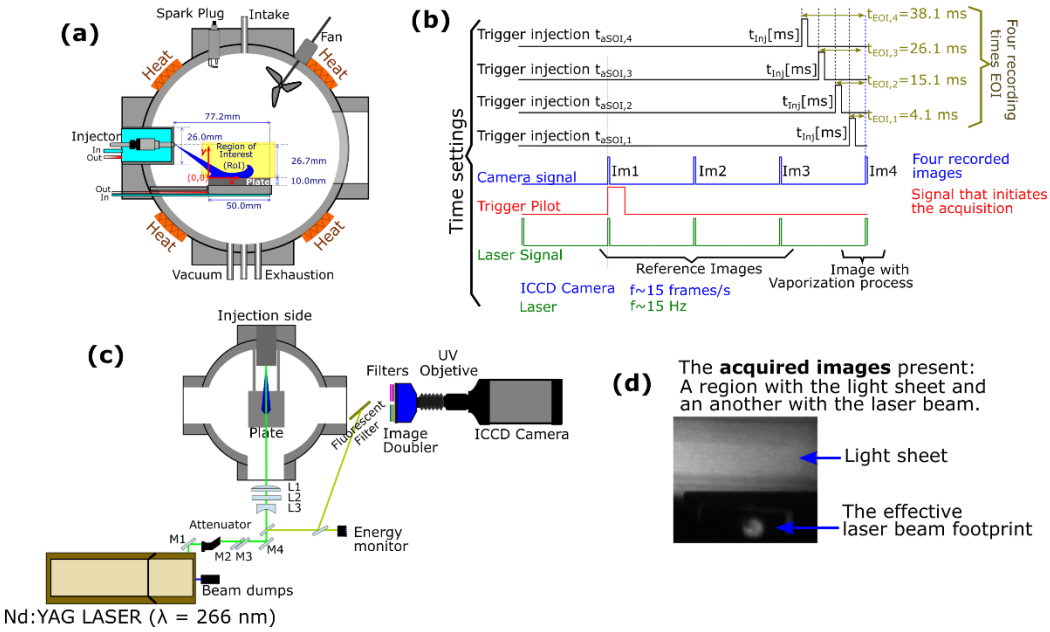

Figure 1. Schematic illustration of the methodology used to analyse the preferential vaporization: Constant volume vessel (a), acquisition time setting (b), diagnostics setup (c), and row image of one of the channels of the image doubler.

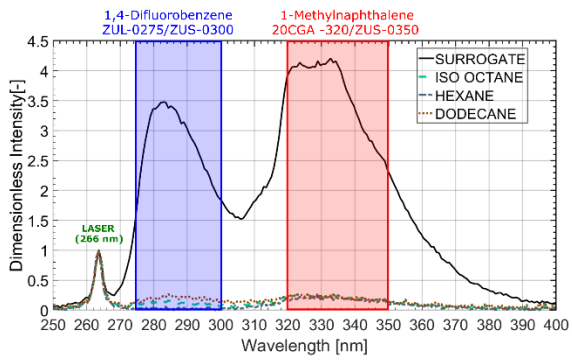

Figure 2. Fluorescence spectra of each component fuel and the surrogate with dopants.

This work is licensed under a Creative Commons 4.0 International License (CC BY-NC-ND 4.0).

Table 1. Experimental conditions

Parameter	Range
Injection pressure	30 / 100 / 200 bar
Initial internal pressure	1.0 bar
Initial internal temperature	90 °C
Plate temperature	80 / 120 / 160 / 200 °C
Injector temperature	80°C
Initial equivalence ratio (ϕ_0)	0.96
Total equivalence ratio (ϕ_{total})	0.98
Injection timing	2.0 / 2.5 / 5.2 ms
Mass of injected fuel	10.23 mg (approx.)

Table 2. Composition of the gasoline surrogates and physical properties of each component (at 25 °C and 1.01325 bar)

Component	Chemical formula	Gasoline surrogate vol%	Density [kg/m3]	B. P. [°C]	E. V. [kJ/kg]
Hexane	C_6H_{14}	10.3	656	68.73	365.5
Iso-octane	C_8H_{18}	78.6	690	99.24	305.5
Dodecane	$C_{12}H_{26}$	11.1	745	216.33	361.2

Table 3. Physical properties of tracers (at 25 °C and 1.01325 bar)

Tracer	Chemical formula	Surrogate fuel vol%	Density [kg/m3]	B. P. [°C]	E. V. [kJ/kg]
1,4-Difluorobenzene (DFB)	$C_6H_4F_2$	0.032	1162	88.8	313.8
1-Methylnaphthalene (1-MN)	$C_{11}H_{10}$	0.08	1016	244.69	438.8

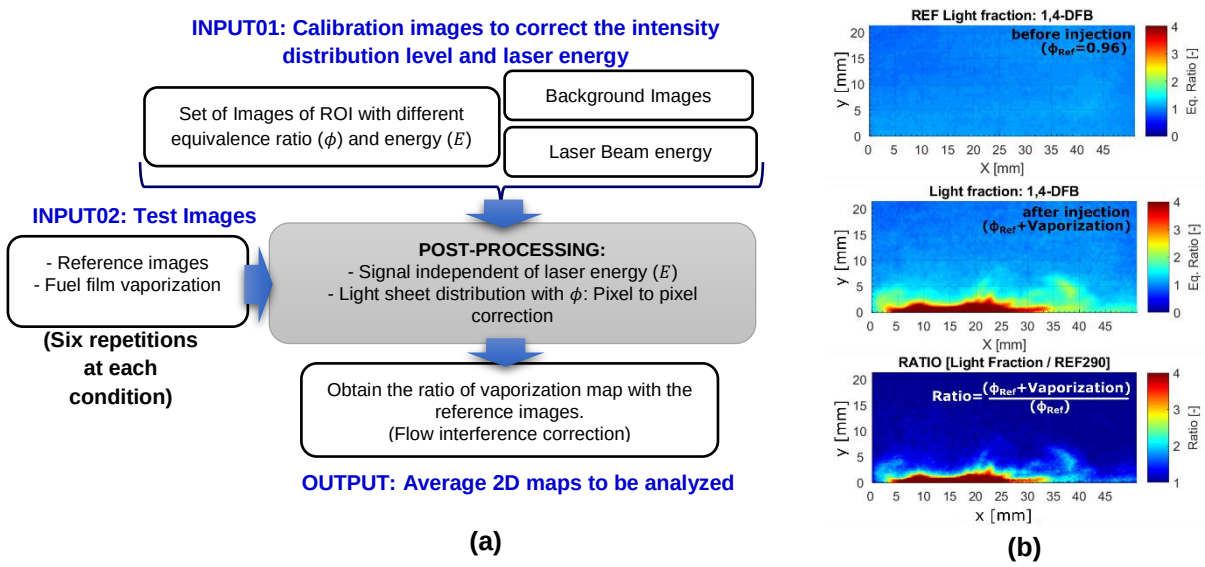

Figure 3. Main steps for Post-processing sequence (a) and 2D Maps of reference average, vaporization and their ratio (b)

Results and discussion

As discussed in the previous section, Figure 4 shows the analysis with the ratios of the average values of the vaporization images with the reference images with an injection pressure of 30 bar. In order to have a general description of the vaporization phenomena two regions (ROI1 and ROI2) were selected. On this way to observe

This work is licensed under a Creative Commons 4.0 International License (CC BY-NC-ND 4.0).

clearly the gradient of concentration of each fraction along *y*-axis, an average value was obtained following the equation 1:

$$\text{Avg Ratio along } \mathbf{x}|_{\mathrm{y}} = \frac{\sum_{\mathrm{x}} \mathrm{Ratio_ROI(x,y)}}{\mathrm{Nx}} \tag{1}$$

Where $\sum_{\mathrm{x}} \mathrm{Ratio_ROI(x,y)}$ is the summation of the ratio values along *x*-axis at a fixed value of *y* and Nx is the number of pixels inside ROI considered along *x*-axis. It is important to recognize ROI1 corresponds to the impingement region and ROI2 is the vortex generation region during the injection and where redepositing droplets take place [13]. The location of these ROIs is presented at the bottom of this Figure. The obtained values are plotted for the four selected times (t_{aSOI}) and for all considered temperatures (T_{wall}). As expected, the values (for light and heavy fractions) far of the surface tend to one because at those distances the effect of the film vaporization does not perturb the initial premix concentration ($\phi_0 = 0.96$) for each fraction. The values start to increase at different heights (*y*-axis); this is represented with green lines. The comparison between curve trends for both regions shows a different behavior, mainly at 160 °C. The preferential vaporization of one fraction respect to other can be observed and the trend values at the different pressures and temperatures will be discussed in detail for the impingement region (ROI1).

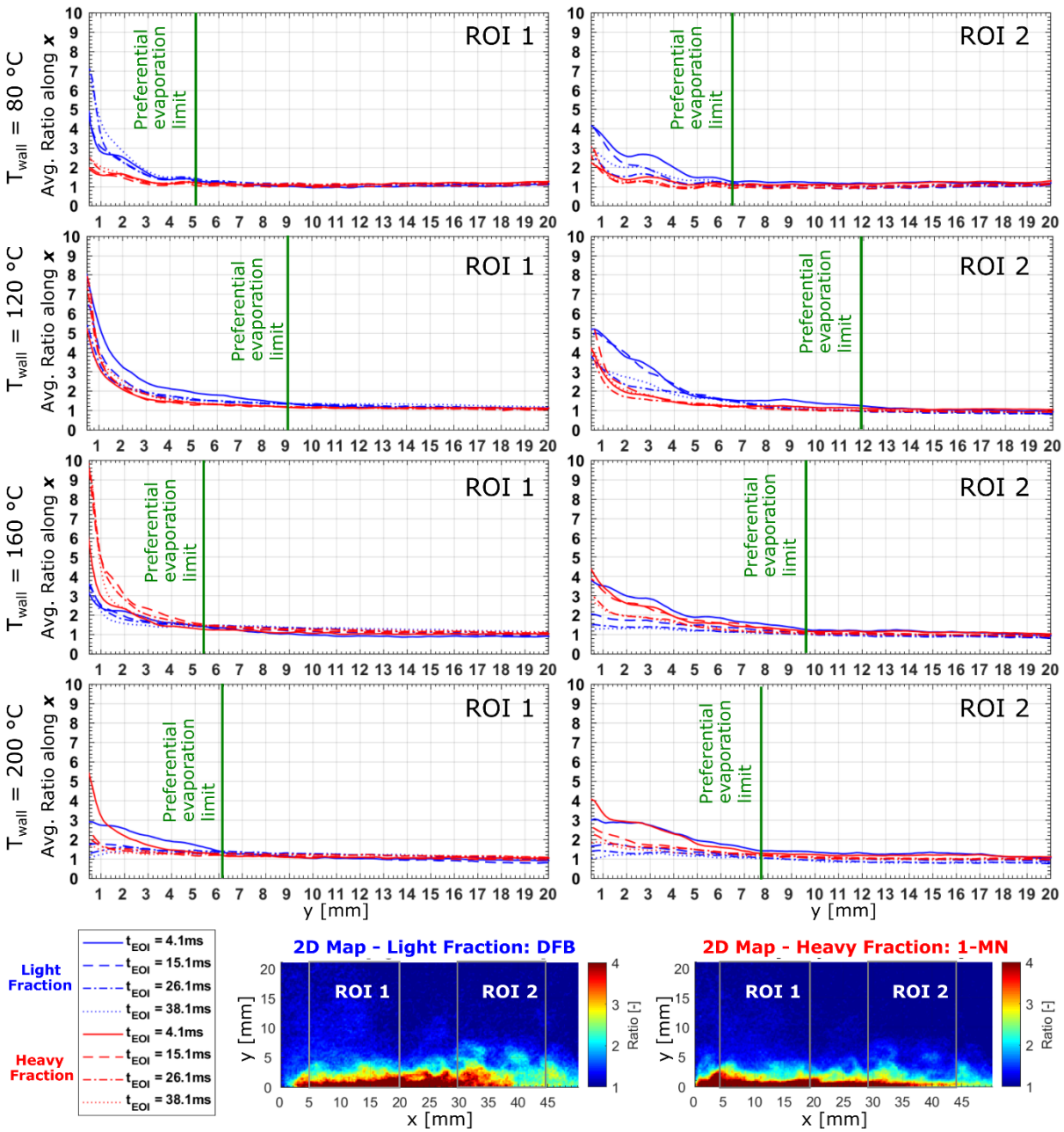

Figure 4. Mean ratio along x for the ROI1 and ROI2 at $\boldsymbol{P_{Inj} = 30\ bar}$

This work is licensed under a Creative Commons 4.0 International License (CC BY-NC-ND 4.0).

Figure 5 shows the same values plotted in the Figure 4 but including the other injection pressures. The *y*-axis was limited to the height of 4 mm. Analysing the plots of the first row at 80 °C at different pressures is possible to see the presence of preferential vaporization where the light fraction vaporize faster of the heavy fraction. This can be explained due the physical properties (boiling point and enthalpy of vaporization). The heavy fraction represented for the dodecane presents a BP (boiling point) up to 200 °C (Table 2), and presented a low vaporization because its ratio values remain constant with the pressure and time. On the other hand, the light and medium fraction (Hexane and Iso-Octane) presented higher vaporization. The injection pressure did not present a high influence on its vaporization behaviour; independent of the final quantity retained in the fuel film, which can change with the injection pressure, the vaporization of the fractions is almost of the same magnitude, with a considerable decrease at 200bar. At this condition (80 °C), as the time increase more fuel is vaporized, the black arrow facing up indicates it. At T_{wall} = 120 °C, comparing the vaporization of both fractions at 30 bar, it is possible to see the preferential vaporization along the timing variation. There is a continuous fall in the ratio values of the light fraction with the time. For the heavy fraction, the vaporization continues to increase with the time. When the injection pressure rose to 100 bar, there is a considerable fall in the vaporization signal of the light fraction, but the behaviour with the time is maintained. At this pressure, the heavy fraction curves are up the light fraction that means that higher vaporization in favour of the heavy respect to the light fraction. At 200 bar, the values for both fraction present the same magnitude compared to 100 bar case, and the same trend with the timing. The main reason of the change in the timing trend from an increase to a decrease (inversion, between 80 and 120°C) can be associated to evaporation rate of the light fraction at those temperatures. The spray droplets content light-medium fractions, which have Nukiyama temperatures (T_N) for pure components in the range from 120 to 140°C. T_N is characterized for presenting the minimum lifetime of droplets when interact with hot surfaces and can be vaporized quickly. As the pressure is increased, the preferential vaporization in favour of heavy fraction is observed. At T_{wall} = 160 °C, the biggest production of heavy vapour is obtained, which increase with the injection pressure. The lower values for the light fraction from 4.1 ms are due the high evaporation rates, at this condition, which vaporized almost everything in the initial instants. The increase of the vaporization process of the heavy fraction with the pressure can be associated to the variation in the composition of the fuel film, which could present a higher concentration of heavy fraction respect to the light fraction because more of the light fraction could be vaporized during the injection period or before the acquisition time. Finally, at T_{wall} = 200 °C, it is possible to see the trend inversion for the curves of the heavy fraction with the timing; the same pattern observed at 120 °C for the light-medium fraction. This can be associated to the faster vaporization of the fuel film, at this temperature (200 °C), which is close to the dodecane BP. The ratio values of the curves fall quickly from 4.1 to 15.1 ms. This could indicate almost complete vaporization of the fuel before the flame front arrival at 38.1 ms [8].

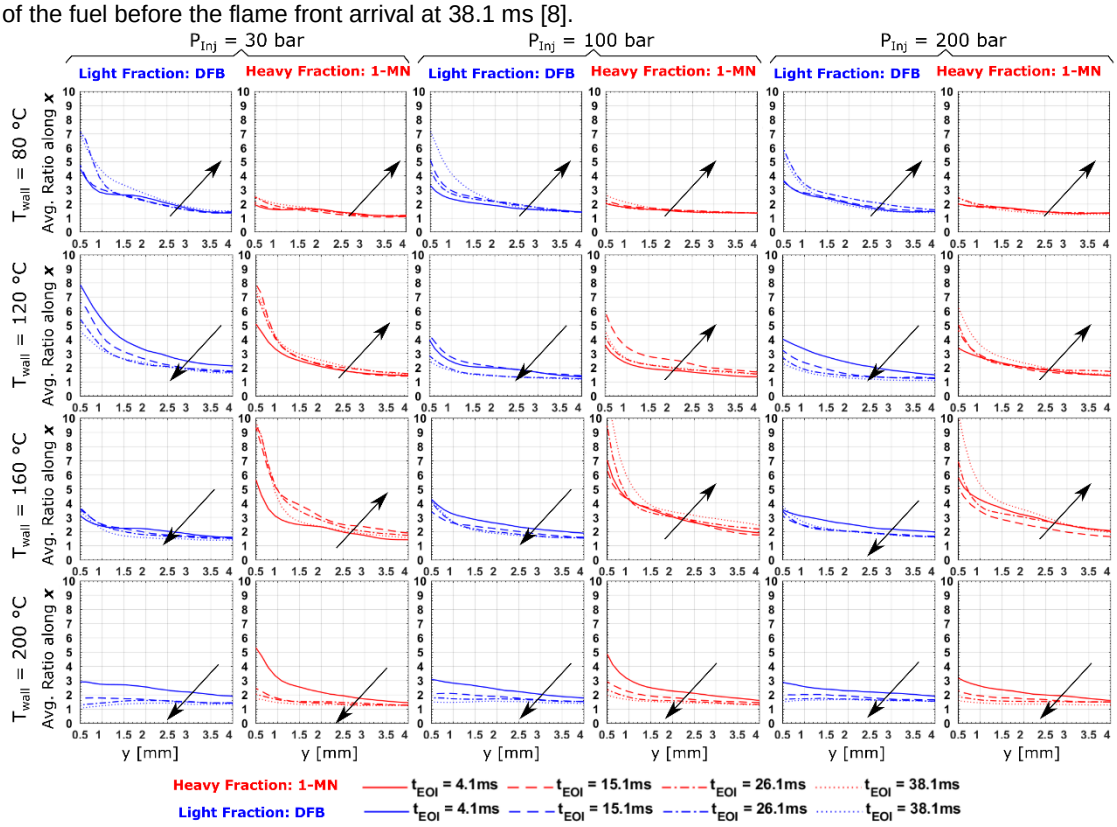

Figure 5. Average ratio for light and heavy fractions at P_{inj} equal to 30, 100 and 200 bar; ROI1

This work is licensed under a Creative Commons 4.0 International License (CC BY-NC-ND 4.0).

Figure 6 shows the mean values of all ratio values of the ROI1 (from 5 to 20 mm, along *x*) but until a height of 4 mm. This Figure analyse the region with big variations due to the vaporization. At 30 bar, it is possible to see the decrease of the light fraction as the temperature increase. The behaviour of the heavy fraction is different, because starts with a small value (constant at 80 °C), and when the temperature increase a maximum can be reached. If the increase continue the values fall at 200 °C. Additionally, it is possible to observe the inversion of the curve trend with the time between 80 and 120 °C for the light fraction and from 180 to 200 °C for the heavy fraction, as found in the Figure 5. At 100 bar of injection pressure, the behaviour is similar and the inversion point respect to the time are observed at the same range of temperature for the light and heavy fractions. The same behaviour is observed for the curves at 200 bar. On this way, the vaporization process of the fuel film generated depend more of the wall temperature than the pressure of injection.

The preferential vaporization to the light fraction is evident just at 80 °C for all injection pressures. At 120 °C, the ratio of the light fraction fall quickly to a value that not change a lot with the time, but the vaporization of the heavy fraction started to rise with the time. A peak of vaporization of the heavy fraction respect to the light components was found in 160 °C for all the injection pressures. From 160 to 200 °C, it is possible to observe the same behaviour described for the light fraction between 80 and 120 °C. The ratio values fall quickly from 4.1 to 15.1 ms, and stayed relatively constant over analysis period. This was explained for a fast vaporization of the heavy components, at these conditions. The maximum evaporation of the heavy part should occur above 200 °C, close to the BP of dodecane (216 °C) but our results showed that it happens to 160 °C, and at 200 °C almost everything was vaporized. This behaviour could be explained by the change in the saturated vapor line due to interaction between components, leading to the components with a higher BP starting to be evaporated at lower temperatures [14].

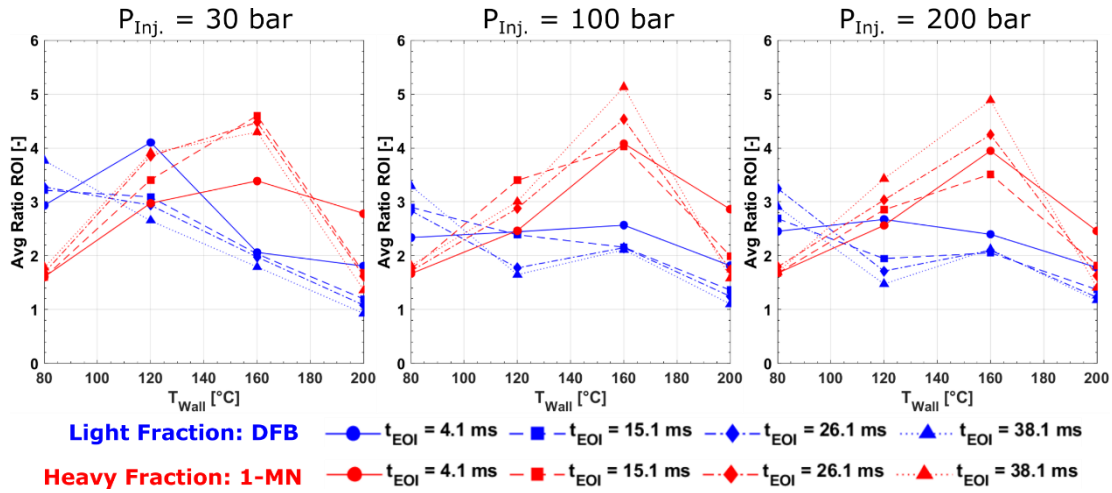

Figure 6. Average ratio for the impingement region (along *x*-axis, from 5 to 20 mm) and a height equal to (*y*) 4 mm, for light and heavy fractions, at 30, 100 and 200 bar; ROI1

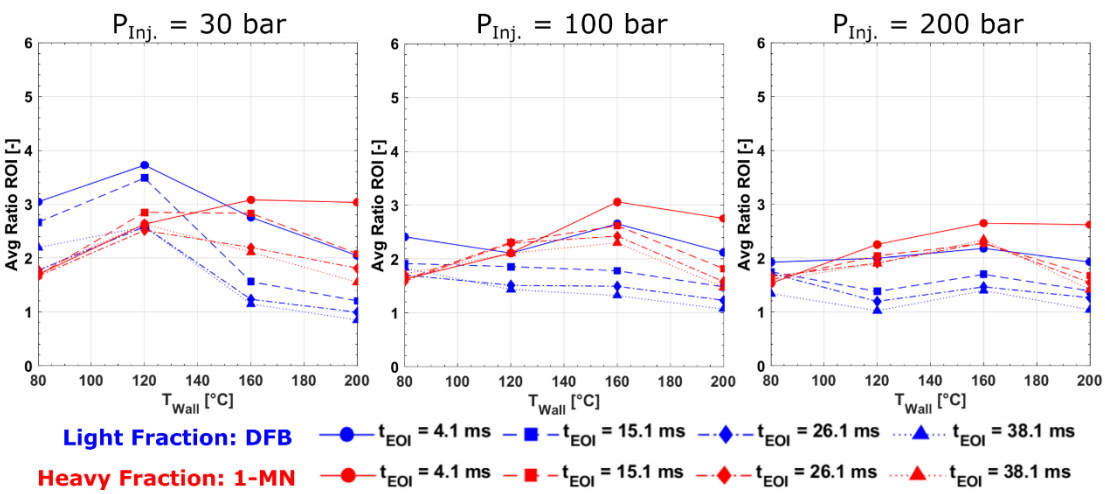

Figure 7. Average ratio for the vortex region (along *x*-axis, from 30 to 45 mm) and a height (*y*) equal to 4 mm, for light and heavy fractions, at 30, 100 and 200 bar; ROI2

This work is licensed under a Creative Commons 4.0 International License (CC BY-NC-ND 4.0).

Whereas the Figure 7 presents the average values for the ROI2 (from 30 to 45 mm along X-axis) until a height of 4 mm. It shows at first glance that the average values are lower than the values presented in the Figure 6, which correspond to the impingement region. This could be associated to a lower mass of liquid to be vaporized in the vortex region. Another feature to be highlighted is the values distribution, which narrows as the pressure increase; the vaporization process can be more sensitive to changes in the injection pressure for this region. At 80 °C, the vaporization was lower and independent of the pressure increase for the heavy fraction. The values of the light fraction fall as the time increase, this behaviour was found in all temperatures tested. For injection pressures of 100 and 200 bar, the values of the light fraction are almost independent of the wall temperature, just the heavy fraction continues sensitive to the wall temperature. T_{wall} = 120 °C presented an interesting behaviour because the quantity of vaporization remains constant in the time, for the heavy fraction. Up to this temperature (160 and 200 °C), the high fraction values start to fall with the time and this behaviour is similar to the one found at 200 °C for in the impingement region (ROI1).
The time at 38.1 ms was defined as the moment when the flame front is close to interact with the fuel film of the wall surface in previous works [8,12]. On this way, in function of the result found for the impingement region, is possible to infer that at T_{wall} = 80 °C, the pool fires generated comes from the both fractions. For 120 °C the pool fires comes from the heavy fraction mainly. With a T_{wall} = 160 °C, the heavy fraction can be burned better, as result of the high vaporization observed. At T_{wall} = 200 °C, the high vaporization rates for both fraction will not permit the generation of pool fires.

Conclusions

The preferential vaporization of a fuel film of a multicomponent surrogate was studied when the injection pressure and the wall temperature are changed, under a controlled environment using a CVV. The use of a novel technique, that involve two fluorescent tracers, was used to mark the light and heavy fraction of the surrogate.
The result showed that the vaporization is not considerably affected by the injection pressure inside the impingement region at a wall temperature of 80 °C. For temperature above 120 °C, it was possible to observe the preferential vaporization in favour of the heavy fraction.
The existence of a fast vaporization point for the light and heavy components was identified, which can be located around 100°C and 180°C, respectively. At this point, the vapour production rate started to fall with the time of analysis. Future works will be directed to identify the main parameter that induce this behaviour.
The vaporization process is more dependent of the wall temperature than the injection pressure, inside the impingement region. Considering the vortex region, the effect of the injection pressure can be considered a relevant parameter. Additionally, it was found that there is a higher quantity of fuel retained in the impingement region than the vortex region.
The vaporization result at 38.1 ms, through all conditions, can be associated to production of soot in the pool fires studied in previous works.

Acknowledgements

Financial support from Continental Powertrain (USA) and Central-Val de Loiret Region (France) is gratefully acknowledged.

Nomenclature

BP	Boiling point
CVV	Constant volume vessel
1-MN	1-MethylNaphthalene
DFB	1,4-DifluorBenzene
EOI	End of Injection
EV	Enthalpy of vaporization
GDI	Gasoline direct injection engine
ϕ	Equivalence ratio
ROI	Region of interest
P_{Inj}	Injection Pressure [bar]
T_{wall}	Aluminium wall temperature [°C]
T_N	Nukiyama temperature

References

[1] US Enviromental Protection Agency, 2018, “Light-Duty Automotive Technology, Carbon Dioxide Emissions, and Fuel Economy Trends: 1975 Through 2017”.
[2] The International Council on Clean Transportation, 2018, “European vehicle market statistics 2017/2018”.
[3] R. O’Driscoll, M. E. J. Stettler, N. Molden, T. Oxley, and H. M. ApSimon, 2018, Science of The Total Environment, 621(4), pp. 282–290.

This work is licensed under a Creative Commons 4.0 International License (CC BY-NC-ND 4.0).

[4] K. Miyashita, T. Tsukamoto, Y. Fukuda, K. Kondo, and T. Aizawa, 2016, SAE Technical Paper, 2016-01-2165.
[5] E. Stevens and R. Steeper, 2001, SAE Technical Paper, 2001-01-1203.
[6] A. Montanaro, L. Allocca, M. Lazzaro, and G. Meccariello, 2016, SAE Technical Paper, 2016-01-0863
[7] L. Allocca, M. Lazzaro, G. Meccariello, and A. Montanaro, , 2016, Energy, vol. 108, pp. 93–98.
[8] A. Roque, F. Foucher, W. Imoehl, and J. Helie, 2019, SAE Technical Paper, 2019-01-0251
[9] Y. Kobayashi and M. Arai, 2015, International Journal of Engines, 9(1), pp. 315-321,.
[10] L. M. Itani, G. Bruneaux, A. Di Lella, and C. Schulz, 2015, Proceedings of the Combustion Institute, 35(3), pp. 2915–2922.
[11] M. Bardi, A. Di Lella, and G. Bruneaux, 2019, *Fuel*, 239(3), pp. 521–533.
[12] A. Roque, F. Foucher, Q. Lamiel, B. Imoehl, N. Lamarque, and J. Helie, 2019, submitted to International Journal of Engine Research.
[13] H. Luo, K. Nishida, S. Uchitomi, Y. Ogata, W. Zhang, and T. Fujikawa, 2018, *Fuel*, 234(6), pp. 56–65.
[14] D. Kawano *et al.*, 2003, *SAE Technical Paper*, 2003-01-1838.

This work is licensed under a Creative Commons 4.0 International License (CC BY-NC-ND 4.0).